

NASA  
TP  
1917  
c.1

## NASA Technical Paper 1917

# Cornering Characteristics of the Nose-Gear Tire of the Space Shuttle Orbiter

William A. Vogler and John A. Tanner

LOAN COPY: RETURN TO  
AFWL TECHNICAL LIBRARY  
KIRTLAND AFB, N.M.

OCTOBER 1981





0067693

## NASA Technical Paper 1917

# Cornering Characteristics of the Nose-Gear Tire of the Space Shuttle Orbiter

William A. Vogler  
*Kentron International, Inc.*  
*Hampton, Virginia*

John A. Tanner  
*Langley Research Center*  
*Hampton, Virginia*



National Aeronautics  
and Space Administration

**Scientific and Technical  
Information Branch**

1981

## INTRODUCTION

The Space Shuttle Orbiter is the first space vehicle designed to land like a conventional airplane, and, as such, it is subjected to the same crosswind effects as commercial and military airplanes. As in the case of conventional airplanes, crosswinds during approach and initial rollout phases of the landing are usually manageable because the pilot can maintain directional control by taking advantage of aerodynamic forces. As ground speed is reduced, however, aerodynamic forces become less effective, and the pilot must rely upon differential braking or nose-gear steering to provide the desired spacecraft heading on the runway. The response of the Space Shuttle to nose-gear steering input is defined, in part, by the cornering characteristics of the nose-gear tire; thus, a need exists to establish these cornering characteristics under realistic operating conditions.

The purpose of this paper is to present results of an investigation of the cornering characteristics of the  $32 \times 8.8$  nose-gear tire of the Space Shuttle Orbiter on a dry concrete runway. These characteristics, which included side and drag forces and friction coefficients, aligning and overturning torques, friction-force moment arm, and the lateral center-of-pressure shift, were obtained over a range of yaw angles from  $0^\circ$  to  $12^\circ$  and tire vertical loads from 22 kN (5000 lbf) to 133 kN (30 000 lbf). This range of yaw angles and vertical loads spans the expected envelope of loads and yaw angles to be encountered during Space Shuttle landing operations. The tests were conducted at ground speeds that ranged from 50 to 100 knots (1 knot = 0.5144 m/sec).

## SYMBOLS

Values are given in both the International System of Units (SI) and in the U.S. Customary Units. The measurements and calculations were made in the U.S. Customary Units. Factors relating the two systems are given in reference 1.

$F_d$	drag force parallel to plane of wheel
$F_s$	side force perpendicular to plane of wheel
$F_z$	tire vertical force
$h$	axle height
$M_x$	overturning torque
$M_z$	aligning torque
$q$	friction-force moment arm
$v$	carriage or ground speed
$y_c$	lateral center-of-pressure shift

$\beta$	coefficients of curve-fitting equations
$\mu_d$	drag-force friction coefficient, parallel to plane of wheel
$\mu_s$	side-force friction coefficient, perpendicular to plane of wheel
$\psi$	tire yaw angle

## APPARATUS AND TEST PROCEDURE

### Test Tires

The tires used in this investigation were 32 × 8.8, type VII, bias-ply aircraft tires of 20-ply rating with a maximum speed rating of 217 knots and a three-groove tread pattern. A photograph of two test tires having new and worn treads is presented in figure 1. The worn tire is shown unmounted and thus unpressurized. The new tire which had an original groove depth of 0.25 cm (0.1 in.) is shown mounted and pressurized. During the course of this investigation, the test tire was changed when the tread was completely worn off and, thus, a total of three tires were used. Throughout the investigation, the tire inflation pressure was maintained at the nominal operational pressure of 2.07 MPa (300 psi).

### Test Facility

The investigation was performed on the 48 000 kg (106 000 lbm) test carriage at the Langley Aircraft Landing Loads and Traction Facility described in reference 2. Figure 2 is a photograph of the carriage with the test-wheel assembly installed, and figure 3 is a close-up view of the tire and wheel mounted within the instrumented dynamometer used to provide accurate measurements of the tire-ground forces.

For the tests described in this paper, approximately 122 m (400 ft) of the available 366 m (1200 ft) of the flat concrete runway was used to provide cornering data. The concrete surface in the test area had a light broom finish in the transverse direction that provided an average texture depth of 159  $\mu\text{m}$  (0.00626 in.), slightly less than that of a typical operational runway. The test runway was level (no crown) and, for all tests, the surface was kept dry.

### Instrumentation

Tire friction forces were measured with the dynamometer shown in figure 3 and illustrated schematically in figure 4. Strain gages were mounted on the five dynamometer support beams: two of the beams were used to measure vertical forces, two were used for measuring drag forces parallel to the wheel plane, and a single beam was used to measure side force perpendicular to the wheel plane. Three accelerometers on the test-wheel axle provided information for inertia corrections to the force data. An electronic interval timer provided a measure of the carriage speed. A slide-wire potentiometer was used to obtain a measure of drop carriage displacement and indirectly to provide a measure of axle height. All data outputs were fed into signal conditioning equipment and then into a frequency-modulated tape recorder.

### Test Procedure

The testing technique consisted of rotating the dynamometer and wheel assembly to the preselected yaw angle, propelling the test carriage to the desired speed, lowering the tire onto the dry runway and applying the selected vertical load, and recording the outputs from the on-board instrumentation. The yaw angle of the wheel assembly, held constant for each test run, ranged from 0° to 12° in 2° increments with additional tests at a yaw angle of 1°. The nominal carriage speeds ranged from about 43 to 104 knots and were measured when the maximum vertical load was attained. Tire vertical loading was varied hydraulically through a range from zero to 147 kN (33 000 lbf) and then back to zero during the course of a typical run, and the loading rate was approximately 133 kN/sec (30 000 lbf/sec).

### Data Reduction

All data were recorded on analog magnetic tape filtered to 1000 Hz. The analog data were then processed through a low pass filter (cutoff frequency of 60 Hz), digitized at 250 samples per second, and used to generate time-history plots for data analysis. From these digitized data, direct measurements were obtained of the drag force (sum of two drag beams), the side force, the vertical force applied to the tire (sum of two vertical beams), the vertical displacement of the drop carriage, and the vertical, drag, and side accelerations of the dynamometer. The instantaneous vertical-, drag-, and side-force data were corrected for acceleration effects and combined as necessary to compute both the instantaneous drag-force friction coefficient parallel to the plane of the wheel and the side-force friction coefficient perpendicular to the plane of the wheel. The load transfer between the two drag-force beams (see fig. 4) provided a measure of the aligning torque about the vertical or steering axis of the wheel. The load transfer between the two vertical-force beams (again see fig. 4) provided a measure of the overturning torque about the axis mutually perpendicular with the vertical and rotation axes. The lateral center-of-pressure shift of the vertical-load pressure distribution due to yawed rolling was defined by

$$y_c = (M_x - hF_s)/F_z \quad (1)$$

where  $h$  was the height of the axle above the runway surface. The friction-force moment arm  $q$  (see ref. 3 for definition) due to yawed rolling was defined by the equation

$$q = M_z / \sqrt{F_d^2 + F_s^2} \quad (2)$$

A least-squares fairing technique (see ref. 4) was used to smooth the digitized data from each run. In this application, seventh-order polynomial line segments were fitted to the data where each line segment was faired through 40 data points with a 10-point overlap between each segment. Linear interpolation was used to insure a smooth transition between line segments within each overlap region, and eight line segments were necessary to fair the data for each second of test duration. The effect of this smoothing routine was to limit the frequency response of the data to 24 Hz without introducing the phase shifts associated with electronic filters.

The influence of the fairing technique on the data from a typical run is illustrated in figure 5. Figures 5(a) and 5(b) are time histories of the unsmoothed and smoothed side force, respectively, and figures 5(c) and 5(d) are time histories of the unsmoothed and smoothed vertical force, respectively. The side force is plotted as a function of the vertical force in figure 5(e) before smoothing and in figure 5(f) after smoothing. The various cornering characteristics from each run were plotted as a function of vertical force, and discrete data points were chosen at pre-selected vertical-force values (dashed vertical lines in fig. 5(f)) to establish the influence of parameter variations on tire cornering characteristics.

#### RESULTS AND DISCUSSION

Data from the yawed-rolling tests conducted on the nose-gear tire of the Space Shuttle Orbiter are presented in table I together with the corresponding test conditions. For purposes of discussion, these data are also presented in figures 6 to 13. The tests examined the effects of three parameters - tire vertical load, yaw angle, and ground speed - on the characteristics of side and drag forces, aligning and overturning torques, friction-force moment arm, and lateral center-of-pressure shift. The data are presented in the form of carpet plots to illustrate functional relationships between the characteristics and the test parameters. In the carpet plots, each characteristic is presented as a function of both vertical load and yaw angle, and the ground speed is identified by test-point symbols. Lines of constant load and constant yaw angle were then fitted to the data in a weighted least-squares fashion to serve as an interpolation aid. The coefficients of bicubic interpolation equations for each characteristic are presented in table II. A glossary of terms used in the study of tire mechanical properties is presented in reference 3. Subsequent paragraphs discuss in detail the effects of tire vertical load, yaw angle, and ground speed on the cornering characteristics of the Space Shuttle nose-gear tire.

##### Side Force

The effect of the test parameters on the developed side force  $F_s$  is presented in figure 6 where the side force is measured normal to the wheel plane (as opposed to cornering force which is measured normal to the direction of motion). When yaw angle is held constant, side force increases with increasing vertical load and generally reaches a maximum at vertical loads between 89 kN (20 000 lbf) and 133 kN (30 000 lbf). This figure also shows that the effect on side force due to changes in the vertical load become more pronounced as yaw angle is increased. As expected, increasing yaw angle while holding vertical load constant increases the side force regardless of the vertical load. At low vertical loadings, however, the side force appears to reach a maximum around the maximum yaw angle tested. No discernible trends are evident with variations in ground speed. Frequently, during high-yaw-angle tests, the lower vertical-load test points are reached in the loading process before the tire has fully spun up. When this condition exists, the side force and other cornering characteristics are negligibly small (see fig. 5(f), for example), and these data were not included in this report.

Since side-force data are generally presented in dimensionless form, they were divided by the respective vertical load on the tire. This process yielded, by definition, side-force friction coefficients  $\mu_s$ , which are presented in the carpet plot of figure 7. For fixed yaw angles, there is a decrease in  $\mu_s$  with increasing vertical load. The figure also shows that for most fixed vertical loads,  $\mu_s$  increases

as the yaw angle is increased. For the lightly loaded tire (44.5 kN (10 000 lbf)), a peak value in  $\mu_s$  of 0.57 is observed at approximately 8° which is in close agreement with the value of 0.60 predicted by equation (88) in reference 5. As the tire vertical load increases, the yaw angle for maximum  $\mu_s$  increases; and for tire vertical loads greater than 89 kN (20 000 lbf), the peak in  $\mu_s$  is reached at yaw angles which are beyond the range tested in this investigation. Again, no trends due to variation in ground speed are evident. These trends are similar to the trends observed in reference 3.

#### Drag Force

The effect of the test parameters on the developed drag force  $F_d$  is presented in figure 8 where the drag force is measured parallel to the wheel plane. When the yaw angle is held constant, drag force generally increases with tire vertical load. Increasing the yaw angle while holding the vertical load constant generally decreases the drag force. For the lightly loaded case (44.5 kN (10 000 lbf)), a minimum drag force is observed around 8°; and for the heavily loaded case (133 kN (30 000 lbf)), a peak drag force is observed at approximately 6°. Dividing the drag force by the respective tire vertical load produces the drag-force friction coefficient  $\mu_d$ , and values of this coefficient are presented in figure 9. These coefficients represent rolling resistance values, and their absolute values are usually below 0.05. Considerable scatter is observed in the data for small yaw angles (less than 2°), and no discernible trends are established in this yaw-angle range. For fixed yaw angles between 4° and 12°,  $\mu_d$  increases with increasing vertical load. When the vertical load is held constant,  $\mu_d$  generally decreases when the yaw angle is increased from 4° to 12°. For the 66.7-kN (15 000-lbf) vertical load case, a minimum  $\mu_d$  value is observed between 10° and 12°; and for the heavily loaded case, a maximum  $\mu_d$  value is observed between 4° and 6°. No trends due to variation in the ground speed are observed for either  $F_d$  or  $\mu_d$ .

#### Aligning Torque

Aligning torque  $M_z$  is defined as the torque developed about the steering axis of a yawed tire. Positive  $M_z$  is considered self-aligning; that is, it tends to reduce yaw angle. Aligning torques for the Shuttle Orbiter nose-gear tire are presented in figure 10. The figure shows that when the yaw angle is held constant, aligning torque generally increases with increasing vertical load. This trend is reversed for the lightly loaded tire at high yaw angles. When vertical load is held constant and yaw angle is increased from zero, aligning torque increases rapidly, reaches a maximum, and then decreases with further increases in yaw. For several conditions, specifically when the tire was lightly loaded and at high yaw angles, the torque is negative; that is, no longer self-aligning. In general, the aligning torque appears to reach a maximum value at yaw angles between 2° and 6°. Figure 10 also shows that aligning torque is insensitive to variations in ground speed. These trends are consistent with data from references 3 and 6.

#### Oversettning Torque

The torque which tends to tilt the wheel plane away from the vertical is referred to as overturning torque  $M_x$ . The carpet plot of figure 11 shows the effects that vertical load and yaw angle have on  $M_x$  over a range of ground speed. At small yaw angles (less than 4°) the overturning torque reaches peak values for

tire vertical loads between 89 kN and 133 kN (20 000 lbf and 30 000 lbf); at higher yaw angles the overturning torque increases with increasing vertical load. Figure 11 also shows that, as expected, an increase in yaw angle at a fixed vertical load increases the overturning torque and that the rate of increase generally increases as the vertical load becomes larger. These trends are similar to those reported in reference 4. As in the case of the other characteristics, there appears to be no discernible effects due to ground-speed variations.

#### Friction-Force Moment Arm

The friction-force moment arm  $q$  is the distance from the friction-force resultant vector to the steering axis and is considered positive when the friction force acts along a line behind the steering axis. The friction-force resultant vector and moment arm represent a force system which is statically equivalent to the actual forces and moments in the footprint. Friction-force moment arms computed from the data of these tests are plotted in figure 12 to show the effect of the various test parameters. The moment arm increases with increasing vertical load on the tire and generally decreases with increasing yaw angle. The moment arm is insensitive to ground-speed variations. At high yaw angles and at light loads,  $q$  is negative, as expected, since the aligning torque (fig. 10) is negative at these test conditions.

#### Center-of-Pressure Shift

Little information is available in the literature on lateral movement of the center of pressure in the tire footprint under yawed-rolling conditions because of the severe instrumentation demands to acquire that parameter. However, measurements of the lateral center-of-pressure shift  $y_c$  were obtained in this investigation and are presented in figure 13 as a function of vertical load and yaw angle. For yaw angles below  $8^\circ$ ,  $y_c$  appears to be fairly insensitive to variations in the vertical load; and for yaw angles above  $8^\circ$ ,  $y_c$  appears to increase with increasing vertical load. As the yaw angle is increased from  $0^\circ$ ,  $y_c$  increases rapidly, but the rate of increase reduces at the higher yaw angles. For the lightly loaded case, a peak in  $y_c$  is observed at a yaw angle of about  $8^\circ$ . Once again,  $y_c$  appears to be insensitive to ground-speed variations. The variation of  $y_c$  with yaw angle and its insensitivity to ground-speed changes are consistent with the data of reference 3.

#### CONCLUDING REMARKS

An experimental investigation was conducted to evaluate the cornering characteristics of the  $32 \times 8.8$  nose-gear tire of the Space Shuttle Orbiter. Data were obtained on a dry concrete runway at nominal ground speeds ranging from 50 to 100 knots and over a range of tire vertical loads and yaw angles which span the expected envelope of loads and yaw angles to be encountered during Space Shuttle landing operations. The cornering characteristics investigated included side and drag forces and friction coefficients, aligning and overturning torques, friction-force moment arm, and the lateral center-of-pressure shift.

The results of this investigation indicate that the cornering characteristics of the Space Shuttle nose-gear tire are insensitive to variations in ground speed over the range tested. The effects on cornering characteristics of variations in the tire

vertical load and yaw angle are as expected. Trends observed are consistent with trends observed during previous cornering tests involving other tire sizes.

Langley Research Center  
National Aeronautics and Space Administration  
Hampton, VA 23665  
August 13, 1981

#### REFERENCES

1. Standard for Metric Practice. E 380-79, American Soc. Testing & Mater., c.1980.
2. Tanner, John A.: Fore-and-Aft Elastic Response Characteristics of 34 x 9.9, Type VII, 14 Ply-Rating Aircraft Tires of Bias-Ply, Bias-Belted, and Radial-Belted Design. NASA TN D-7449, 1974.
3. Tanner, John A.; Stubbs, Sandy M.; and McCarty, John L.: Static and Yawed-Rolling Mechanical Properties of Two Type VII Aircraft Tires. NASA TP-1863, 1981.
4. Alfaro-Bou, Emilio; and Vaughan, Victor L., Jr.: Light Airplane Crash Tests at Impact Velocities of 13 and 27 m/sec. NASA TP-1042, 1977.
5. Smiley, Robert F.; and Horne, Walter B.: Mechanical Properties of Pneumatic Tires With Special Reference to Modern Aircraft Tires. NASA TR R-64, 1960. (Supersedes NACA TN 4110.)
6. Tanner, John A.; and Dreher, Robert C.: Cornering Characteristics of a 40 x 14-16 Type VII Aircraft Tire and a Comparison With Characteristics of a C40 x 14-21 Cantilever Aircraft Tire. NASA TN D-7351, 1973.

TABLE I.- SUMMARY OF TEST CONDITIONS AND TIRE CORNERING CHARACTERISTICS

V, knots	$\psi$ , deg	F <sub>z</sub>		F <sub>s</sub>		F <sub>d</sub>		M <sub>z</sub>		M <sub>x</sub>		Y <sub>c</sub>		q	
		kN	lbf	kN	lbf	kN (a)	lbf	N-m	in-lbf	N-m	in-lbf	cm (a)	in.	cm (a)	in.
50	0	22.24	5000	0.00	0	****N/A****		224.0	1982	-356	-3147	****N/A****		****N/A****	
		44.48	10000	.59	132	****N/A****		472.8	4185	-89	-787	****N/A****		****N/A****	
		66.72	15000	.20	44	****N/A****		298.6	2643	-444	-3933	****N/A****		****N/A****	
		88.96	20000	.98	220	****N/A****		373.3	3304	-89	-787	****N/A****		****N/A****	
51	0	22.24	5000	.41	93	****N/A****		435.5	3855	187	1652	****N/A****		****N/A****	
		44.48	10000	.82	185	****N/A****		383.3	3392	249	2203	****N/A****		****N/A****	
		66.72	15000	.96	216	****N/A****		592.3	5242	373	3304	****N/A****		****N/A****	
		88.96	20000	.96	216	****N/A****		540.0	4780	187	1652	****N/A****		****N/A****	
		111.21	25000	.96	216	****N/A****		487.8	4317	0	0	****N/A****		****N/A****	
		133.45	30000	1.23	278	****N/A****		487.8	4317	187	1652	****N/A****		****N/A****	
78	0	22.24	5000	0.00	0	****N/A****		298.6	2643	-267	-2360	****N/A****		****N/A****	
		44.48	10000	.39	88	****N/A****		373.3	3304	-178	-1573	****N/A****		****N/A****	
		66.72	15000	.20	44	****N/A****		547.5	4846	0	0	****N/A****		****N/A****	
		88.96	20000	.98	220	****N/A****		398.2	3524	89	787	****N/A****		****N/A****	
		111.21	25000	.98	220	****N/A****		423.1	3744	267	2360	****N/A****		****N/A****	
		133.45	30000	.98	220	****N/A****		448.0	3965	-267	-2360	****N/A****		****N/A****	
104	0	22.24	5000	.20	44	****N/A****		124.4	1101	-178	-1573	****N/A****		****N/A****	
		44.48	10000	.59	132	****N/A****		224.0	1982	0	0	****N/A****		****N/A****	
		66.72	15000	.78	176	****N/A****		248.9	2203	0	0	****N/A****		****N/A****	
		88.96	20000	.78	176	****N/A****		273.8	2423	178	1573	****N/A****		****N/A****	
		111.21	25000	.98	220	****N/A****		273.8	2423	-178	-1573	****N/A****		****N/A****	
		133.45	30000	.98	220	****N/A****		248.9	2203	0	0	****N/A****		****N/A****	
43	1	44.48	10000	4.51	1013	2.69	604	373.3	3304	1600	14160	-.13	-.05	7.16	2.82
		66.72	15000	6.27	1410	1.46	327	497.7	4405	2311	20453	.13	.05	7.67	3.02
		88.96	20000	7.64	1718	2.69	604	647.0	5727	2933	25960	.33	.13	7.80	3.07
		111.21	25000	8.23	1850	4.31	969	796.4	7048	2933	25960	.23	.09	8.56	3.37
		133.45	30000	7.64	1718	3.08	692	945.7	8370	2844	25173	.28	.11	11.38	4.48
75	1	22.24	5000	3.14	705	.17	38	273.8	2423	1155	10227	-.15	-.06	8.43	3.32
		44.48	10000	5.09	1145	1.96	441	448.0	3965	1778	15733	0.00	0.00	8.56	3.37
		66.72	15000	7.25	1630	2.52	566	572.4	5066	2666	23600	.20	.08	7.54	2.97
		88.96	20000	7.84	1762	2.69	604	746.6	6608	2933	25960	.28	.11	9.19	3.62
		111.21	25000	7.84	1762	4.26	957	871.0	7709	2755	24386	.15	.06	9.60	3.78
		133.45	30000	7.64	1718	4.20	944	995.5	8811	2755	24386	.20	.08	11.51	4.53
100	1	22.24	5000	3.14	705	.28	63	273.8	2423	1155	10227	0.00	0.00	8.05	3.17
		44.48	10000	5.49	1233	1.01	227	448.0	3965	2044	18093	-.05	-.02	8.05	3.17
		66.72	15000	7.64	1718	2.13	478	547.5	4846	2844	25173	.20	.08	7.04	2.77
		88.96	20000	8.23	1850	2.69	604	746.6	6608	3022	26746	.23	.09	8.69	3.42
		111.21	25000	8.03	1806	2.91	654	895.9	7930	2933	25960	.20	.08	10.36	4.08
		133.45	30000	7.84	1762	3.70	831	1020.3	9031	2755	24386	.15	.06	11.76	4.63
52	2	22.24	5000	5.49	1233	.34	76	298.6	2643	2222	19666	.43	.17	5.49	2.16
		44.48	10000	10.39	2335	1.01	227	572.4	5066	4355	38546	1.40	.55	5.49	2.16
		66.72	15000	13.91	3128	1.62	365	821.3	7269	5599	49559	1.17	.46	5.77	2.27
		88.96	20000	16.07	3612	2.24	503	1169.7	10352	6222	55066	1.19	.47	7.67	3.02
		111.21	25000	15.87	3568	2.91	654	1493.2	13216	6399	56639	1.04	.41	9.19	3.62
		133.45	30000	15.09	3392	2.74	617	1742.1	15419	6133	54279	.97	.38	11.13	4.38

<sup>a</sup> Notation N/A refers to data not available.

TABLE I.- Continued

V, knots	$\psi$ , deg	F <sub>Z</sub>		F <sub>S</sub>		F <sub>d</sub>		M <sub>Z</sub>		M <sub>X</sub>		Y <sub>C</sub>		q	
		kN	lbf	kN	lbf	kN	lbf	N-m	in-lbf	N-m	in-lbf	cm	in.	cm	in.
76	2	44.48	10000	10.78	2423	.17	38	472.8	4185	4266	37760	.76	.30	4.22	1.66
		66.72	15000	14.11	3172	1.96	441	796.4	7048	5511	48773	.76	.30	5.36	2.11
		88.96	20000	15.87	3568	3.14	705	1095.0	9692	6133	54279	.99	.39	6.78	2.67
		111.21	25000	16.07	3612	4.42	994	1418.5	12555	6222	55066	.84	.33	8.43	3.32
		133.45	30000	15.09	3392	3.92	881	1692.3	14978	6133	54279	.89	.35	10.49	4.13
101	2	22.24	5000	5.88	1322	1.57	352	273.8	2423	2400	21240	1.07	.42	3.84	1.51
		44.48	10000	10.58	2379	1.01	227	448.0	3965	4355	38546	1.55	.61	4.34	1.71
		66.72	15000	14.30	3216	2.80	629	746.6	6608	5955	52706	1.45	.57	4.98	1.96
		88.96	20000	15.28	3436	3.36	755	1119.9	9912	6133	54279	1.40	.55	7.29	2.87
		111.21	25000	15.87	3568	3.81	856	1443.4	12775	6311	55853	1.17	.46	8.81	3.47
53	4	44.48	10000	18.03	4053	2.74	617	423.1	3744	7288	64506	2.21	.87	2.44	.96
		66.72	15000	25.28	5683	.45	101	671.9	5947	10310	91252	2.36	.93	2.69	1.06
		88.96	20000	29.20	6564	1.74	390	1269.2	11233	12088	106986	2.31	.91	4.34	1.71
		111.21	25000	29.79	6696	2.58	579	1816.7	16079	12443	110132	2.11	.83	6.02	2.37
		133.45	30000	27.83	6256	4.03	906	2488.7	22026	11910	105412	1.96	.77	8.81	3.47
77	4	44.48	10000	20.18	4537	1.12	252	298.6	2643	7999	70799	1.83	.72	1.52	.60
		66.72	15000	26.26	5903	.28	63	746.6	6608	10755	95186	2.31	.91	2.82	1.11
		88.96	20000	29.59	6652	1.90	428	1368.8	12115	11999	106198	2.24	.88	4.60	1.81
		111.21	25000	29.59	6652	3.92	881	2015.8	17841	12088	106986	2.16	.85	6.78	2.67
		133.45	30000	27.63	6211	5.82	1309	2588.2	22907	11910	105412	1.80	.71	8.56	3.37
102	4	66.72	15000	25.67	5771	3.81	856	895.9	7930	10310	91252	2.08	.82	3.58	1.41
		88.96	20000	29.98	6740	3.14	705	1319.0	11674	11732	103839	1.96	.77	4.47	1.76
		111.21	25000	29.79	6696	4.37	982	1791.8	15859	12266	108559	2.08	.82	5.89	2.32
		133.45	30000	29.20	6564	5.21	1171	2488.7	22026	11643	103052	1.83	.72	8.43	3.32
72	6	44.48	10000	22.14	4978	-1.01	-227	-49.8	-441	8621	76306	1.35	.53	-.25	-.10
		66.72	15000	31.55	7093	.06	13	273.8	2423	12710	112492	2.36	.93	.89	.35
		88.96	20000	38.60	8678	.84	189	671.9	5947	15554	137665	2.77	1.09	1.65	.65
		111.21	25000	41.35	9295	3.36	755	1592.7	14097	16621	147105	2.72	1.07	3.84	1.51
		133.45	30000	41.35	9295	4.37	982	2488.7	22026	16710	147892	2.67	1.05	6.02	2.37
75	6	44.48	10000	24.28	5458	1.14	256	505.2	4471	10017	88656	2.95	1.16	2.06	.81
		66.72	15000	31.27	7031	1.18	264	783.9	6938	13252	117291	3.43	1.35	2.51	.99
		88.96	20000	36.35	8172	2.35	529	1550.4	13722	15679	138767	3.63	1.43	4.29	1.69
		111.21	25000	37.04	8326	3.64	819	2247.3	19890	15865	140419	3.38	1.33	6.10	2.40
		133.45	30000	36.21	8141	5.29	1189	2944.1	26057	15741	139317	3.07	1.21	8.15	3.21
104	6	88.96	20000	37.86	8511	1.92	432	940.7	8326	15119	133811	2.24	.88	2.51	.99
		111.21	25000	39.78	8943	2.86	643	1411.1	12489	15990	141520	2.36	.93	3.48	1.37
		133.45	30000	40.05	9004	4.62	1040	2473.7	21894	16736	148128	2.69	1.06	6.17	2.43
101	6	44.48	10000	24.83	5581	-.20	-44	17.4	154	10639	94163	4.04	1.59	0.00	0.00
		66.72	15000	33.47	7524	.55	123	574.9	5088	14372	127203	4.29	1.69	1.70	.67
		88.96	20000	36.49	8203	1.92	432	1149.8	10176	15679	138767	3.84	1.51	3.12	1.23
		111.21	25000	36.90	8295	3.37	758	1985.9	17577	15927	140969	3.58	1.41	5.46	2.15
		133.45	30000	35.12	7894	4.70	1057	2909.2	25749	15430	136564	3.33	1.31	8.23	3.24

TABLE I.- Continued

V, knots	$\psi$ , deg	F <sub>Z</sub>		F <sub>S</sub>		F <sub>D</sub>		M <sub>Z</sub>		M <sub>X</sub>		Y <sub>C</sub>		q	
		kN	lbf	kN	lbf	kN	lbf	N-m	in-lbf	N-m	in-lbf	cm	in.	cm	in.
75	8	44.48	10000	25.24	5674	-.51	-115	-348.4	-3084	9706	85903	1.50	.59	-1.35	-.53
		66.72	15000	34.16	7678	.24	53	-156.8	-1388	13501	119493	2.44	.96	-.46	-.18
		88.96	20000	42.11	9467	.59	132	296.1	2621	17172	151982	3.53	1.39	.71	.28
		111.21	25000	44.58	10022	4.19	943	1254.3	11101	18229	161344	3.51	1.38	2.87	1.13
		133.45	30000	44.72	10053	5.88	1322	2404.0	21278	18665	165198	3.61	1.42	5.28	2.08
79	8	44.48	10000	23.73	5335	.08	18	69.7	617	10203	90308	3.81	1.50	.28	.11
		66.72	15000	34.43	7740	.55	123	191.6	1696	14870	131608	4.50	1.77	.64	.25
		88.96	20000	39.37	8850	1.53	344	609.7	5396	17109	151432	4.60	1.81	1.60	.63
		111.21	25000	42.52	9559	2.90	652	1167.2	10330	18540	164097	4.29	1.69	2.77	1.09
		133.45	30000	42.66	9590	4.51	1013	1985.9	17577	18478	163546	3.84	1.51	4.65	1.83
105	8	88.96	20000	43.62	9806	-.04	-9	104.5	925	17669	156388	3.15	1.24	.18	.07
		111.21	25000	45.40	10207	2.51	564	313.6	2775	18354	162445	3.02	1.19	1.70	.67
		133.45	30000	48.15	10824	2.82	634	1898.8	16806	20469	181167	3.56	1.40	3.58	1.41
100	8	44.48	10000	26.34	5921	-.55	-123	-470.4	-4163	10266	90859	2.06	.81	-1.70	-.67
		66.72	15000	35.53	7987	1.18	264	-209.0	-1850	14248	126101	2.84	1.12	-.53	-.21
		88.96	20000	42.11	9467	3.49	784	226.5	2004	17234	152533	3.58	1.41	.64	.25
		111.21	25000	46.23	10392	2.67	599	1062.7	9405	19038	168502	3.94	1.55	2.24	.88
		133.45	30000	44.85	10084	5.92	1330	2073.0	18348	18727	165749	3.86	1.52	4.57	1.80
101	8	44.48	10000	23.18	5211	1.14	256	52.3	463	10079	89207	4.42	1.74	0.00	0.00
		66.72	15000	35.94	8079	1.41	317	139.4	1233	14932	132159	4.11	1.62	.46	.18
		88.96	20000	42.25	9498	2.78	626	731.7	6476	18043	159692	4.65	1.83	1.70	.67
		111.21	25000	44.99	10115	3.61	811	1655.0	14648	19225	170154	4.72	1.86	3.05	1.20
		133.45	30000	43.62	9806	5.53	1242	2107.9	18656	19038	168502	4.04	1.59	4.83	1.90
74	10	66.72	15000	35.94	8079	1.57	352	-522.6	-4626	14870	131608	3.68	1.45	-1.42	-.56
		88.96	20000	48.15	10824	3.61	811	69.7	617	20034	177313	4.67	1.84	.18	.07
		111.21	25000	52.54	11811	4.70	1057	522.6	4626	22087	195485	4.78	1.88	.99	.39
		133.45	30000	54.04	12150	6.15	1383	1376.2	12181	23082	204295	4.90	1.93	2.51	.99
74	10	66.72	15000	32.37	7278	.59	132	-226.5	-2004	13439	118943	3.28	1.29	-.71	-.28
		88.96	20000	43.07	9683	1.10	247	104.5	925	18478	163546	4.47	1.76	.36	.14
		111.21	25000	49.66	11163	2.59	581	731.7	6476	21402	189427	4.80	1.89	1.42	.56
		133.45	30000	52.40	11780	3.80	855	1550.4	13722	22771	201542	4.88	1.92	3.05	1.20
98	10	66.72	15000	37.31	8388	.16	35	-783.9	-6938	14745	130507	2.87	1.13	-2.16	-.85
		88.96	20000	46.50	10454	1.57	352	-627.1	-5551	19100	169053	4.17	1.64	-1.35	-.53
		111.21	25000	50.48	11348	1.92	432	-296.1	-2621	21216	187775	4.47	1.76	-.64	-.25
		133.45	30000	52.40	11780	4.31	969	592.3	5242	22522	199399	4.78	1.88	1.17	.46
100	10	66.72	15000	33.61	7555	.24	53	-174.2	-1542	14061	124449	3.68	1.45	-.53	-.21
		88.96	20000	42.39	9529	1.21	273	191.6	1696	18292	161894	4.70	1.85	.46	.18
		111.21	25000	45.13	10145	1.92	432	487.8	4317	19723	174559	4.67	1.84	1.07	.42
		133.45	30000	46.50	10454	3.53	793	871.0	7709	20469	181167	4.42	1.74	2.16	.85
76	12	66.72	15000	33.06	7432	.63	141	-261.3	-2313	14061	124449	4.24	1.67	-.81	-.32
		88.96	20000	43.21	9714	1.33	300	-156.8	-1388	18852	166850	5.16	2.03	-.36	-.14
		111.21	25000	52.95	11903	2.43	546	52.3	463	22833	202093	5.31	2.08	.10	.04
		133.45	30000	57.61	12952	3.41	767	574.9	5088	25446	225220	5.82	2.29	.99	.39

TABLE I.- Concluded

V, knots	$\psi$ , deg	F <sub>Z</sub>		F <sub>S</sub>		F <sub>d</sub>		M <sub>Z</sub>		M <sub>X</sub>		Y <sub>C</sub>		q	
		kN	lbf	kN	lbf	kN	lbf	N-m	in-lbf	N-m	in-lbf	cm	in.	cm	in.
99	12	66.72	15000	37.45	8419	1.02	229	-940.7	-8326	15119	133811	3.28	1.29	-2.51	-.99
		88.96	20000	49.11	11040	1.45	326	-801.3	-7093	20220	178965	4.52	1.78	-1.52	-.60
		111.21	25000	57.20	12859	2.27	511	-662.0	-5859	23393	207048	4.70	1.85	-1.07	-.42
		133.45	30000	59.67	13414	4.12	925	69.7	617	24887	220264	4.95	1.95	.10	.04
100	12	66.72	15000	34.29	7709	-.24	-53	-557.5	-4934	14310	126652	3.53	1.39	-1.52	-.60
		88.96	20000	41.97	9436	.90	203	-522.6	-4626	17856	158040	4.11	1.62	-1.17	-.46
		111.21	25000	48.56	10916	1.18	264	-331.0	-2930	21091	186674	4.75	1.87	-.71	-.28
		133.45	30000	53.91	12119	2.98	670	278.7	2467	23393	207048	5.03	1.98	.53	.21

TABLE II.- BICUBIC

$$[\text{Characteristic} = \beta_0 + \beta_1 F_z + \beta_2 F_z^2 + \beta_3 F_z^3]$$

Cornering characteristics		Coefficients of $\beta$ for -				
		$\beta_0$	$\beta_1$	$\beta_2$	$\beta_3$	$\beta_4$
$F_s$ , N (lbf)	SI	$-3.3416 \times 10^3$	$9.4981 \times 10^{-2}$	$-7.8146 \times 10^{-8}$	$-4.0600 \times 10^{-12}$	$3.3435 \times 10^3$
	U.S.	$(-7.5123 \times 10^2)$	$(9.4981 \times 10^{-2})$	$(-3.4761 \times 10^{-7})$	$(-8.0333 \times 10^{-11})$	$(7.5165 \times 10^2)$
$\mu_s$	SI	$-3.1045 \times 10^{-3}$	$2.3555 \times 10^{-7}$	$-3.7580 \times 10^{-12}$	$1.6522 \times 10^{-17}$	$0.16670$
	U.S.	$(-3.1045 \times 10^{-3})$	$(1.0478 \times 10^{-6})$	$(-7.4358 \times 10^{-11})$	$(1.4542 \times 10^{-15})$	$(0.16670)$
$F_d$ , N (lbf)	SI	$9.4574 \times 10^2$	$1.7911 \times 10^{-2}$	$1.9823 \times 10^{-7}$	$-1.5041 \times 10^{-12}$	$-5.8040 \times 10^2$
	U.S.	$(2.1261 \times 10^2)$	$(1.7911 \times 10^{-2})$	$(8.8179 \times 10^{-7})$	$(-2.9762 \times 10^{-11})$	$(-1.3048 \times 10^2)$
$\mu_d$	SI	$3.8969 \times 10^{-2}$	$2.5601 \times 10^{-9}$	$-3.8621 \times 10^{-13}$	$-3.9400 \times 10^{-18}$	$-9.9506 \times 10^{-3}$
	U.S.	$(3.8969 \times 10^{-2})$	$(1.1388 \times 10^{-8})$	$(-7.6418 \times 10^{-12})$	$(-3.4678 \times 10^{-16})$	$(-9.9506 \times 10^{-3})$
$M_z$ , N-m (in-lbf)	SI	$1.9507 \times 10$	$8.2103 \times 10^{-4}$	$-3.2516 \times 10^{-9}$	$-1.9424 \times 10^{-14}$	$1.7663 \times 10^2$
	U.S.	$(1.7265 \times 10^2)$	$(3.2324 \times 10^{-2})$	$(-5.6944 \times 10^{-7})$	$(-1.5131 \times 10^{-11})$	$(1.5633 \times 10^3)$
$M_x$ , N-m (in-lbf)	SI	$-7.9353 \times 10^2$	$3.0389 \times 10^{-2}$	$-1.3274 \times 10^{-7}$	$-7.4122 \times 10^{-13}$	$7.1965 \times 10^2$
	U.S.	$(-7.0233 \times 10^3)$	$(1.1964)$	$(-2.3246 \times 10^{-5})$	$(-5.7741 \times 10^{-10})$	$(6.3694 \times 10^3)$
$y_c$ , cm (in.)	SI	-1.3149	$2.1476 \times 10^{-5}$	$-2.3572 \times 10^{-10}$	$9.3808 \times 10^{-16}$	$8.3236 \times 10$
	U.S.	$(-5.1769 \times 10^{-1})$	$(3.7611 \times 10^{-5})$	$(-1.8363 \times 10^{-9})$	$(3.2506 \times 10^{-14})$	$(3.2770 \times 10^{-1})$
$q$ , cm (in.)	SI	$1.1223 \times 10$	$-7.2742 \times 10^{-5}$	$6.8968 \times 10^{-10}$	$-4.2993 \times 10^{-16}$	-2.9192
	U.S.	$(4.4184)$	$(-1.2739 \times 10^{-4})$	$(5.3726 \times 10^{-9})$	$(-1.4898 \times 10^{-14})$	$(-1.1493)$

aBoundary values of characteristic, 0 when  $F_z = 30\ 000, 25\ 000, 20\ 000, 15\ 000, 10\ 000, 5000$ , and 0 lbf with  $\psi = 0^\circ$ ; and when  $\psi = 1^\circ, 2^\circ, 4^\circ, 6^\circ, 8^\circ, 10^\circ$ , and  $12^\circ$  with  $F_z = 0$  for a total of 14 additional points to weight boundary.

bBoundary values of characteristic, 0 when  $F_z = 30\ 000, 25\ 000, 20\ 000, 15\ 000, 10\ 000$ , and 5000 lbf with  $\psi = 0^\circ$ ; repeated for a total of 167 additional points to weight boundary.

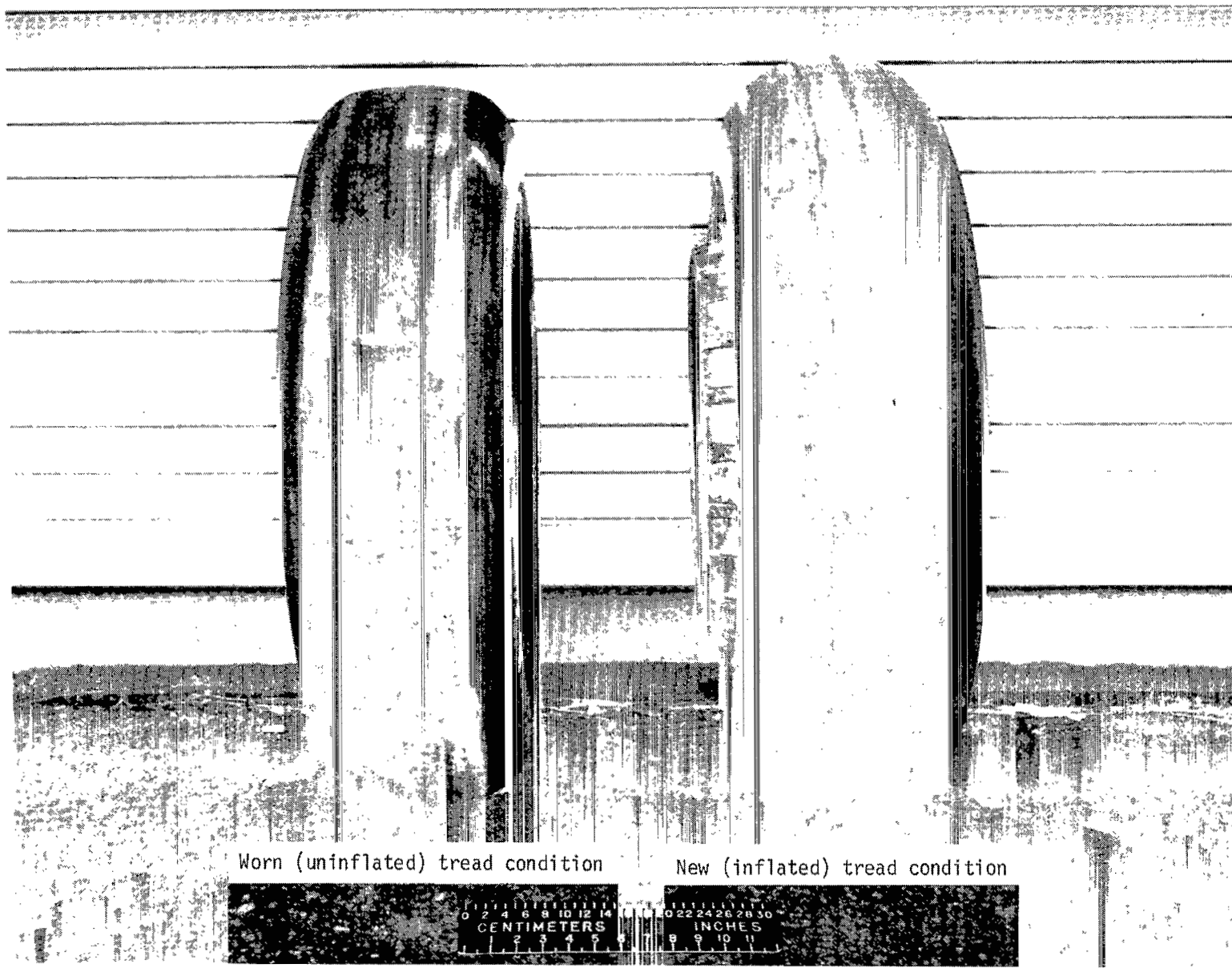
cNo boundary value weighting used.

dBoundary values used in (a) above repeated for a total of 84 additional points to weight boundary.

INTERPOLATION EQUATIONS

$$+ \beta_4 \psi + \beta_5 \psi^2 + \beta_6 \psi^3 + \beta_7 F_z \psi + \beta_8 F_z \psi^2 + \beta_9 F_z^2 \psi]$$

Coefficients of $\beta$ for -					Number of data points used	Boundary condition
$\beta_5$	$\beta_6$	$\beta_7$	$\beta_8$	$\beta_9$		
-4.0866 $(-9.1871 \times 10^{-1})$	9.6513 $(2.1697)$	$6.9333 \times 10^{-2}$ $(6.9333 \times 10^{-2})$	$-9.0677 \times 10^{-4}$ $(-9.0677 \times 10^{-4})$	$-1.6509 \times 10^{-7}$ $(-7.3436 \times 10^{-7})$	139	(a)
$-1.2407 \times 10^{-2}$ $(-1.2407 \times 10^{-2})$	$1.1631 \times 10^{-4}$ $(1.1631 \times 10^{-4})$	$-5.4298 \times 10^{-7}$ $(-2.4153 \times 10^{-6})$	$1.4449 \times 10^{-8}$ $(2.8590 \times 10^{-7})$	$-3.7037 \times 10^{-13}$ $(-3.2598 \times 10^{-11})$	139	(b)
$6.7920 \times 10$ $(1.5269 \times 10)$	$1.0984 \times 10^{-1}$ $(2.4694 \times 10^{-2})$	$-1.0844 \times 10^{-3}$ $(-1.0844 \times 10^{-3})$	$-8.0974 \times 10^{-4}$ $(-8.0974 \times 10^{-4})$	$6.8798 \times 10^{-8}$ $(3.0603 \times 10^{-7})$	117	(c)
$3.3772 \times 10^{-4}$ $(3.3772 \times 10^{-4})$	$1.5060 \times 10^{-5}$ $(1.5060 \times 10^{-5})$	$9.0355 \times 10^{-8}$ $(4.0192 \times 10^{-7})$	$-6.8720 \times 10^{-9}$ $(-3.0568 \times 10^{-8})$	$1.7479 \times 10^{-13}$ $(3.4585 \times 10^{-12})$	117	(c)
$-6.2965 \times 10$ $(-5.5729 \times 10^2)$	4.9674 $(4.3965 \times 10)$	$3.8097 \times 10^{-3}$ $(1.4999 \times 10^{-1})$	$-7.0523 \times 10^{-4}$ $(-2.7765 \times 10^{-2})$	$2.8409 \times 10^{-8}$ $(4.9751 \times 10^{-6})$	139	(b)
$-1.0123 \times 10^2$ $(-8.9600 \times 10^2)$	3.5308 $(3.1250 \times 10)$	$3.5601 \times 10^{-2}$ $(1.4016)$	$-9.2192 \times 10^{-4}$ $(-3.6296 \times 10^{-2})$	$-7.2382 \times 10^{-8}$ $(-1.2676 \times 10^{-5})$	139	(d)
$-9.8064 \times 10^{-2}$ $(-3.8608 \times 10^{-2})$	$9.6713 \times 10^{-4}$ $(3.8076 \times 10^{-4})$	$2.7235 \times 10^{-6}$ $(4.7695 \times 10^{-6})$	$5.1351 \times 10^{-7}$ $(8.9930 \times 10^{-7})$	$-7.6350 \times 10^{-11}$ $(-2.6742 \times 10^{-10})$	117	(c)
$1.8707 \times 10^{-1}$ $(7.3653 \times 10^{-2})$	$-1.5328 \times 10^{-3}$ $(-6.0346 \times 10^{-4})$	$1.6389 \times 10^{-5}$ $(2.8701 \times 10^{-5})$	$-1.2566 \times 10^{-6}$ $(-2.2007 \times 10^{-6})$	$-1.8610 \times 10^{-11}$ $(-1.4497 \times 10^{-10})$	117	(c)



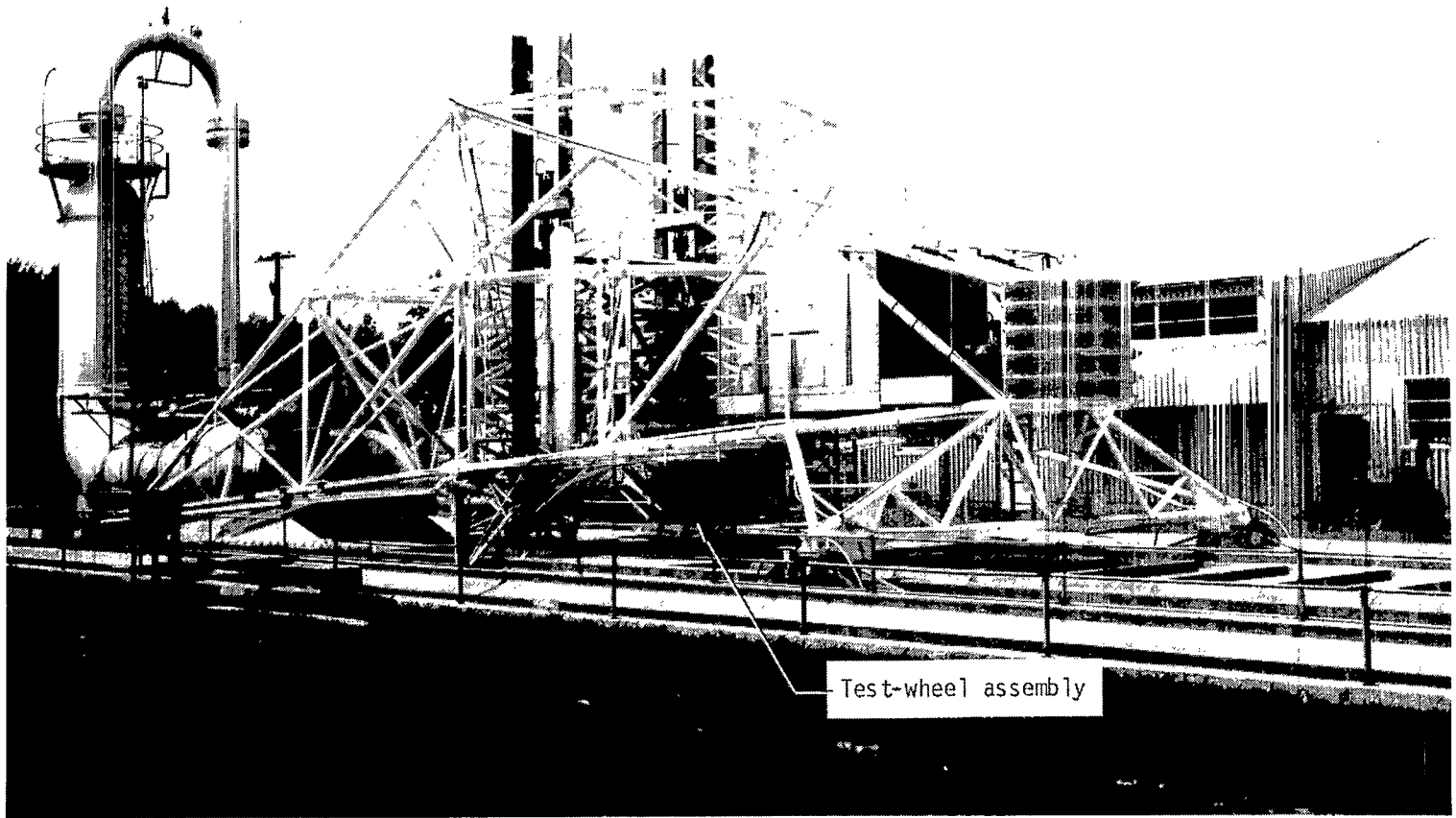
Worn (uninflated) tread condition

New (inflated) tread condition

0 2 4 6 8 10 12 14	0 2 2 4 6 8 10 11
CENTIMETERS	INCHES
2 3 4 5 6 7	8 9 10 11

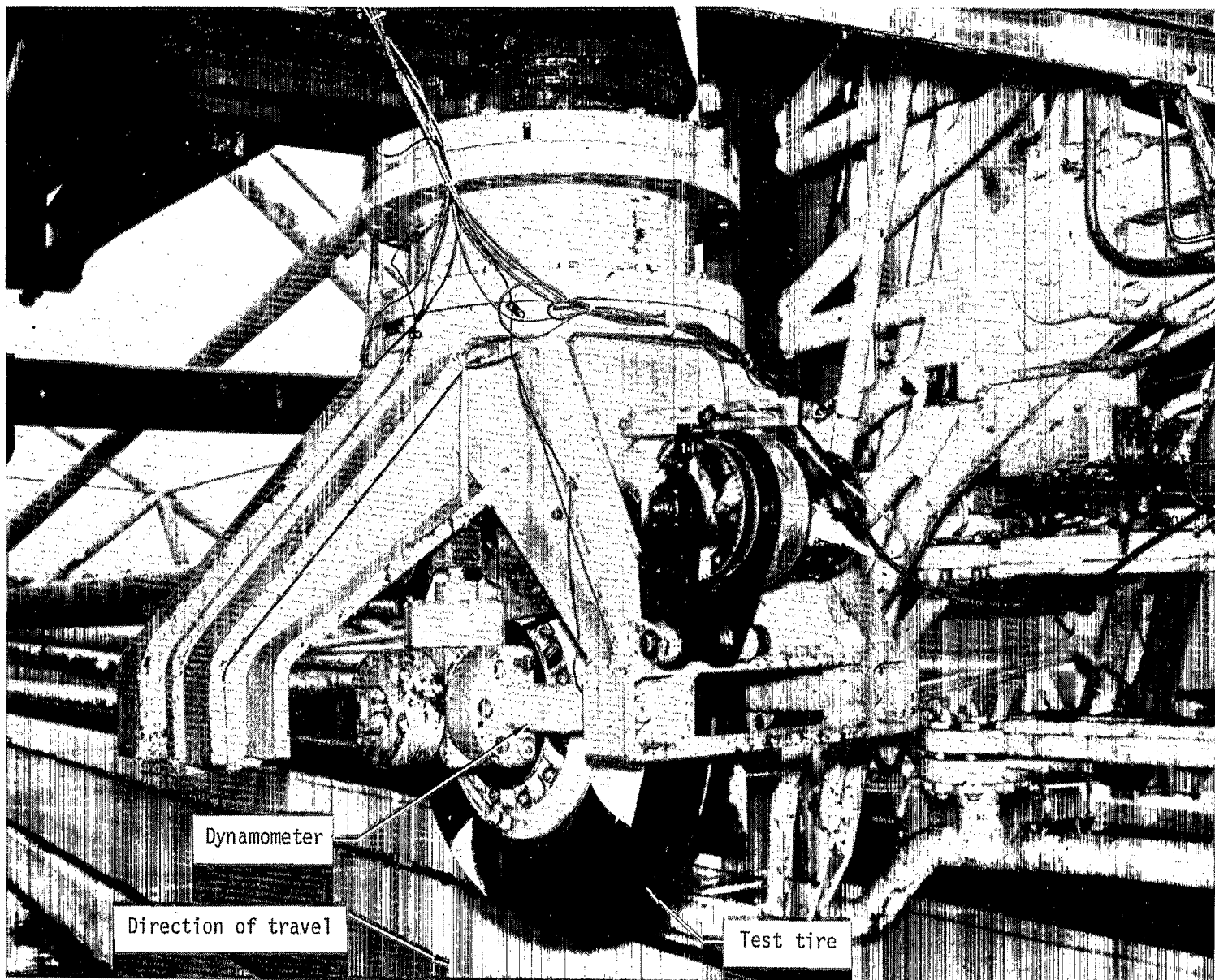
I-81-3256.1

Figure 1.- New and worn tread condition of three-groove, 32 x 8.8, type VII, nose-gear test tire of Space Shuttle.



L-69-5860.2

Figure 2.- Photograph of carriage with test-wheel assembly installed.



L-80-4387.1

Figure 3.- Photograph of test tire and instrumented dynamometer.

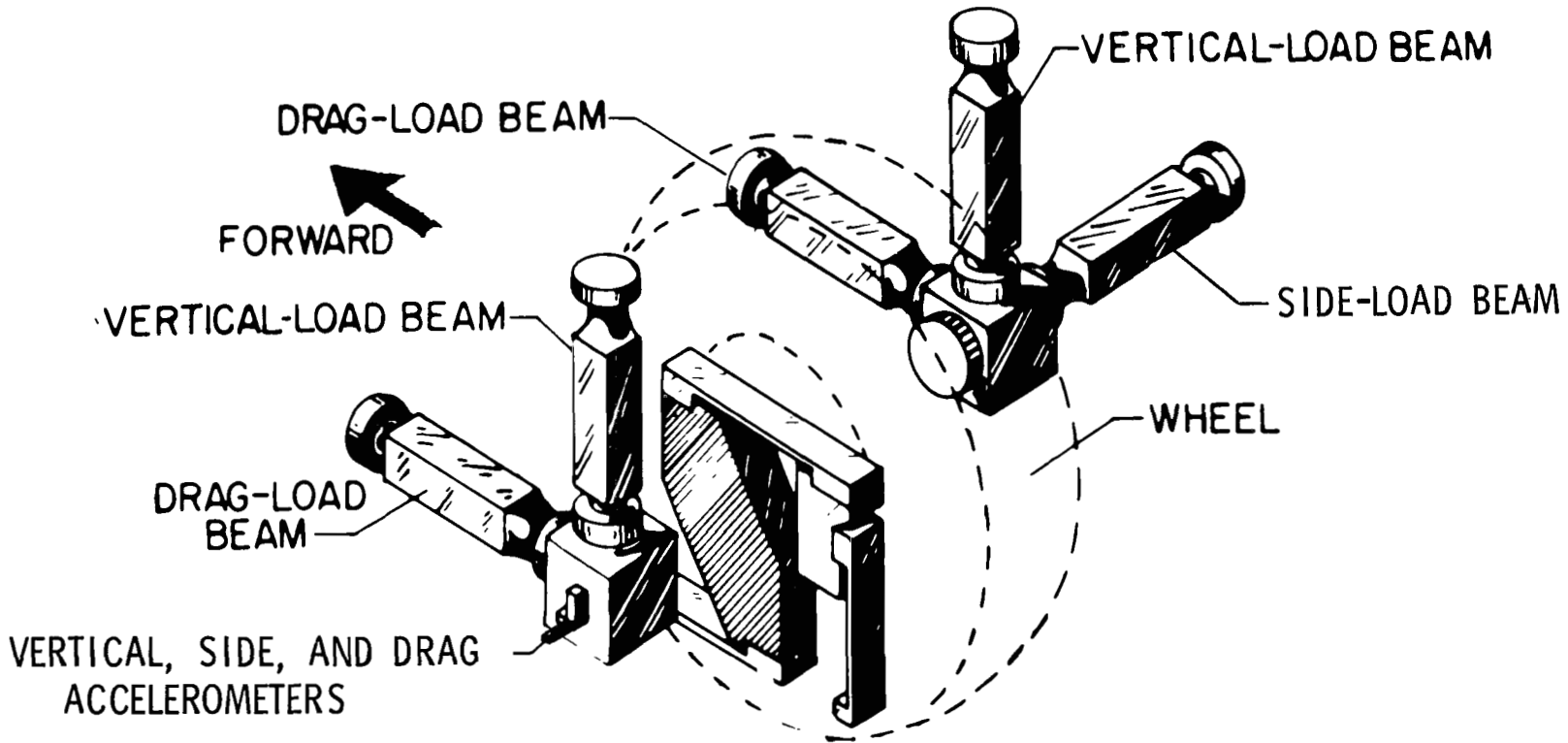


Figure 4.- Schematic drawing of dynamometer details.

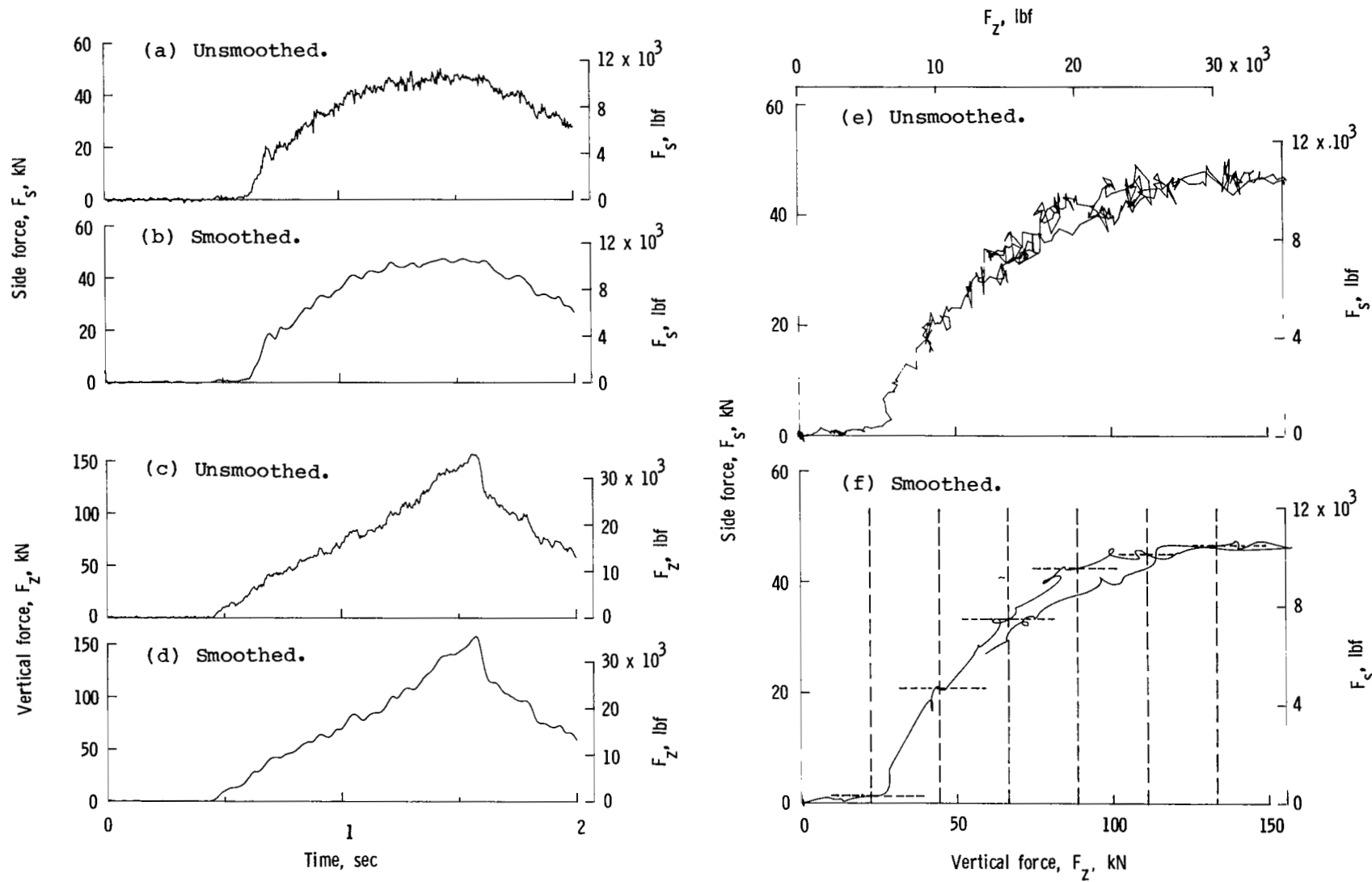


Figure 5.- Data fairing technique. Yaw angle,  $10^\circ$ ; ground speed, 100 knots.

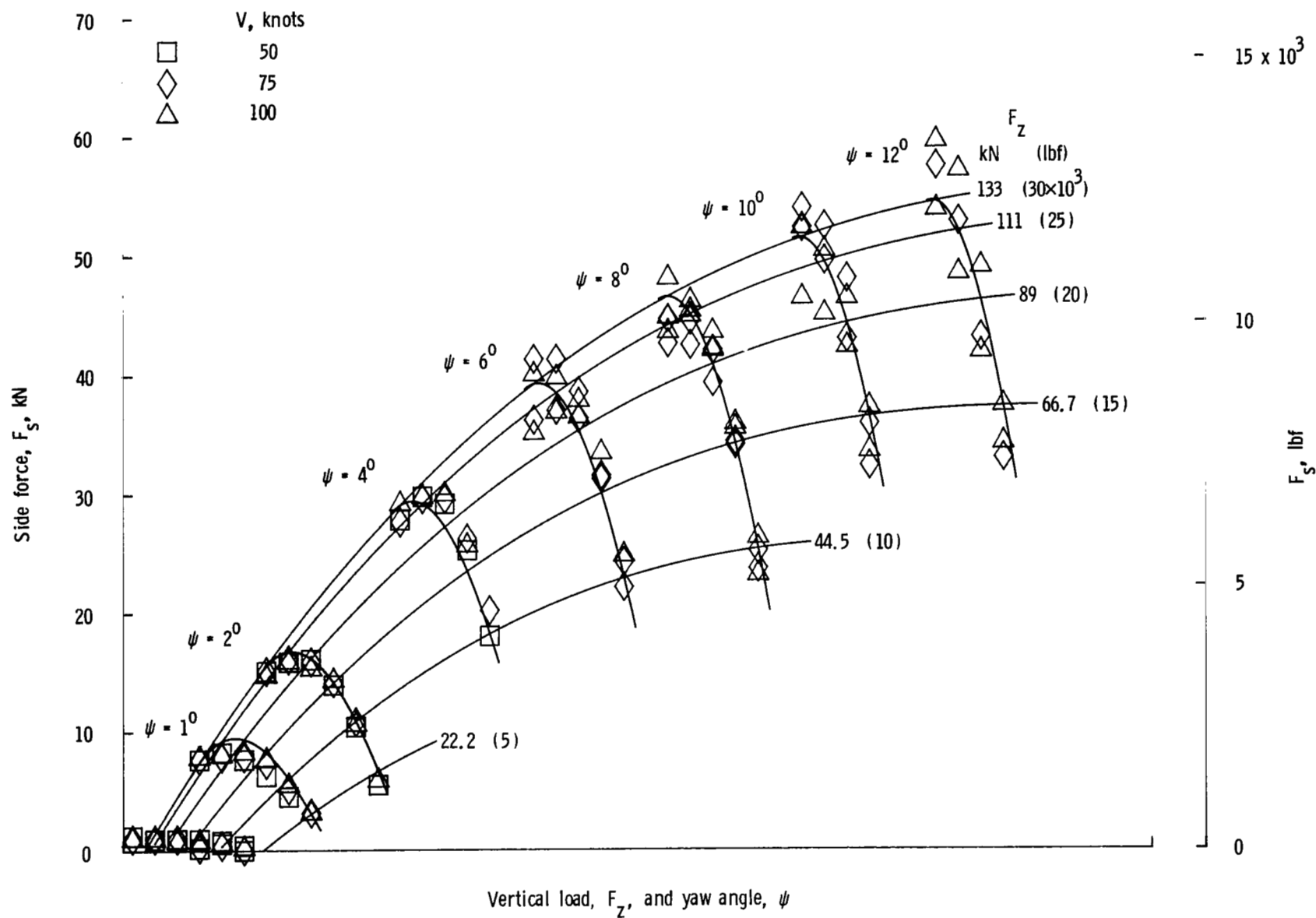


Figure 6.- Variation of side force with vertical load and yaw angle over a range of ground speed.

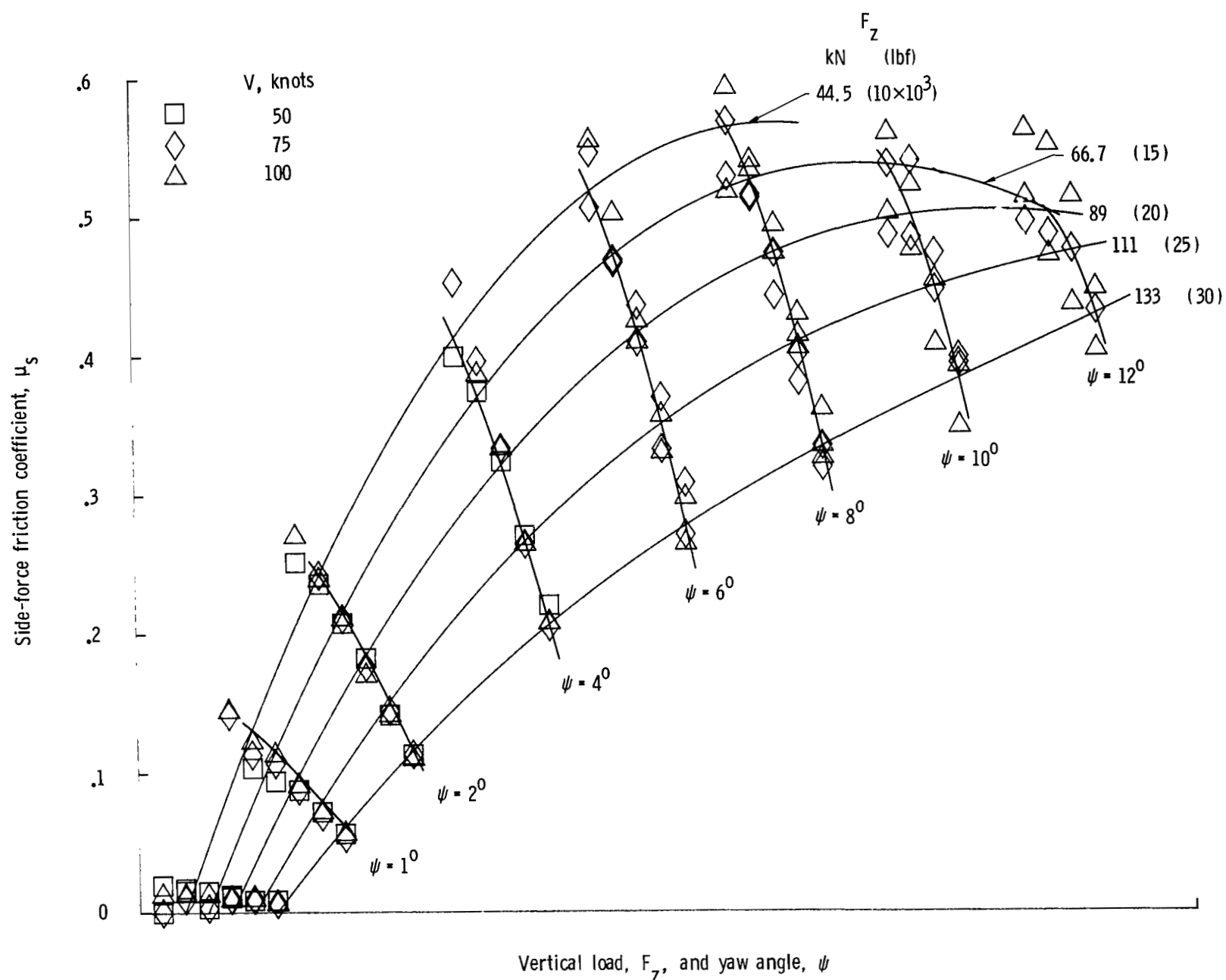


Figure 7.- Variation of side-force friction coefficient with vertical load and yaw angle over a range of ground speed.

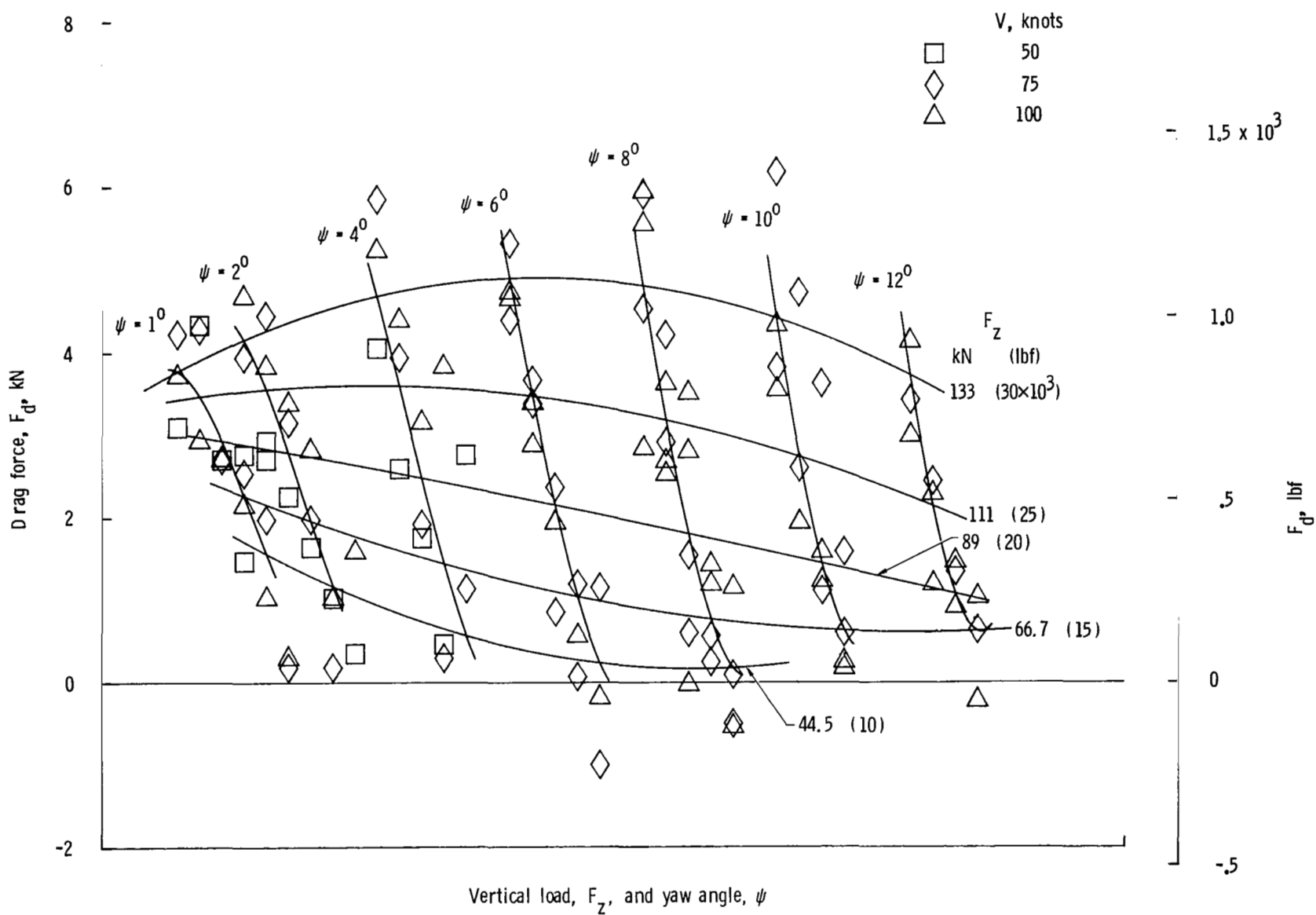


Figure 8.- Variation of drag force with vertical load and yaw angle over a range of ground speed.

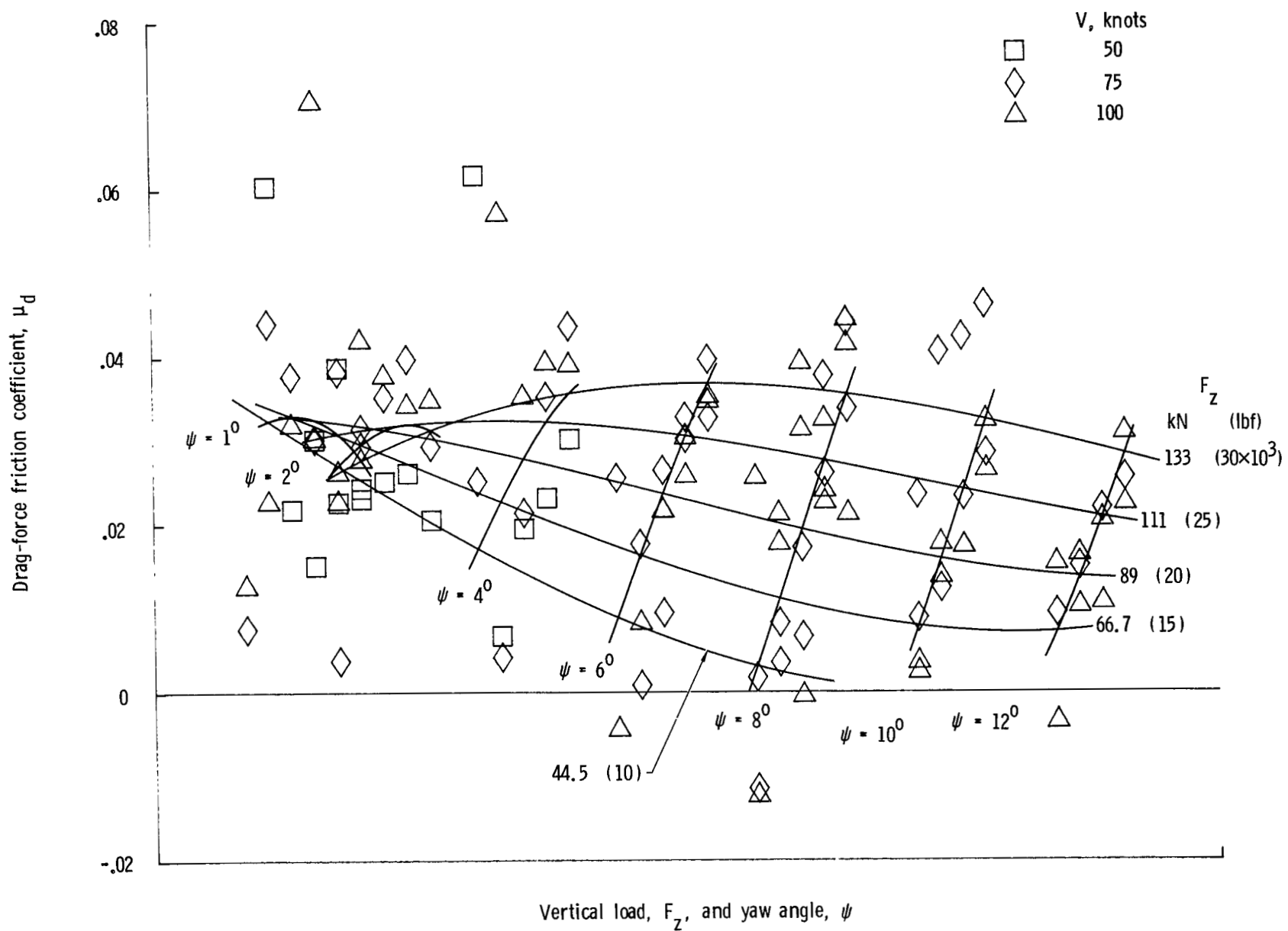


Figure 9.- Variation of drag-force friction coefficient with vertical load and yaw angle over a range of ground speed.

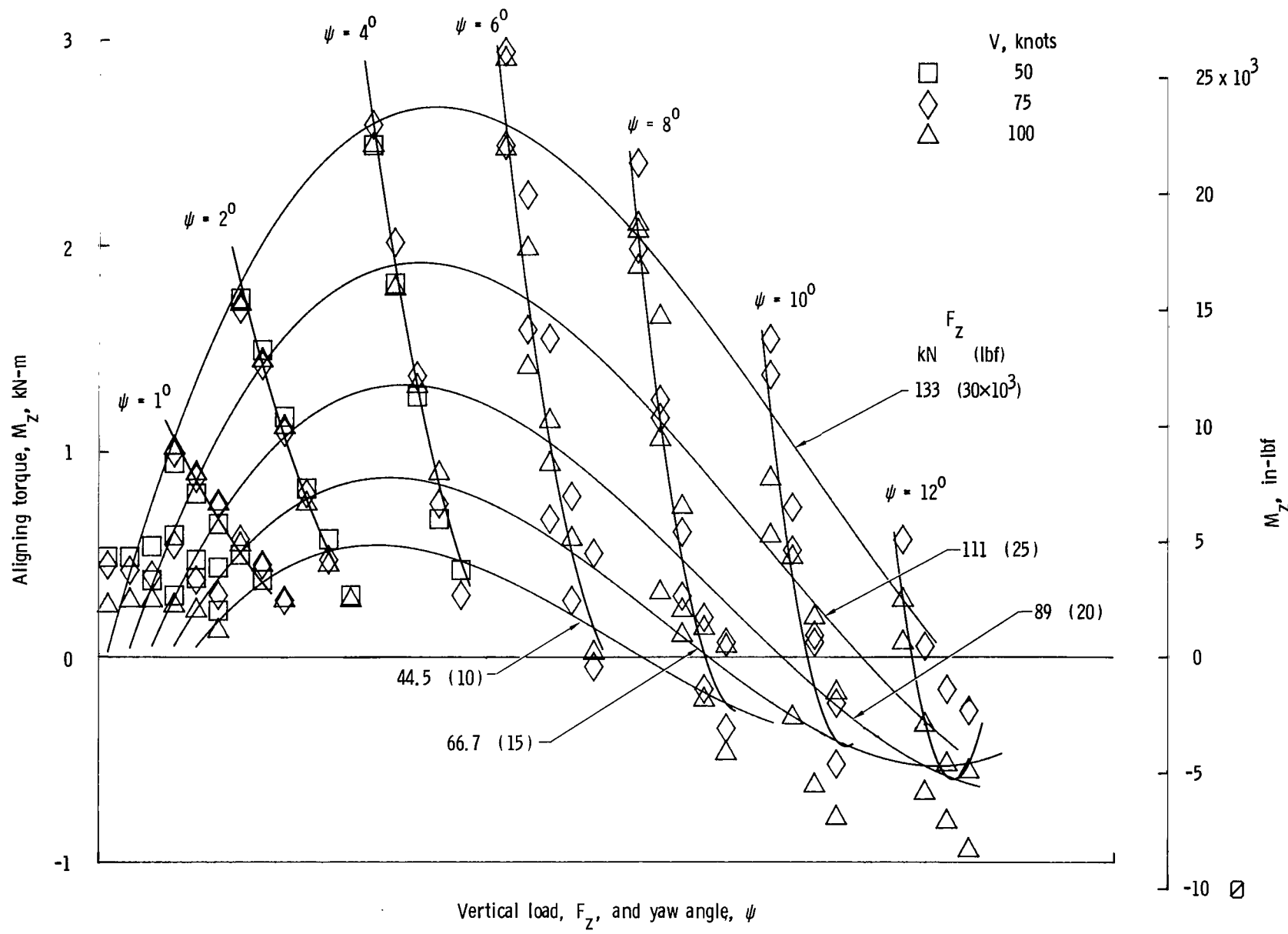


Figure 10.- Variation of aligning torque with vertical load and yaw angle over a range of ground speed.

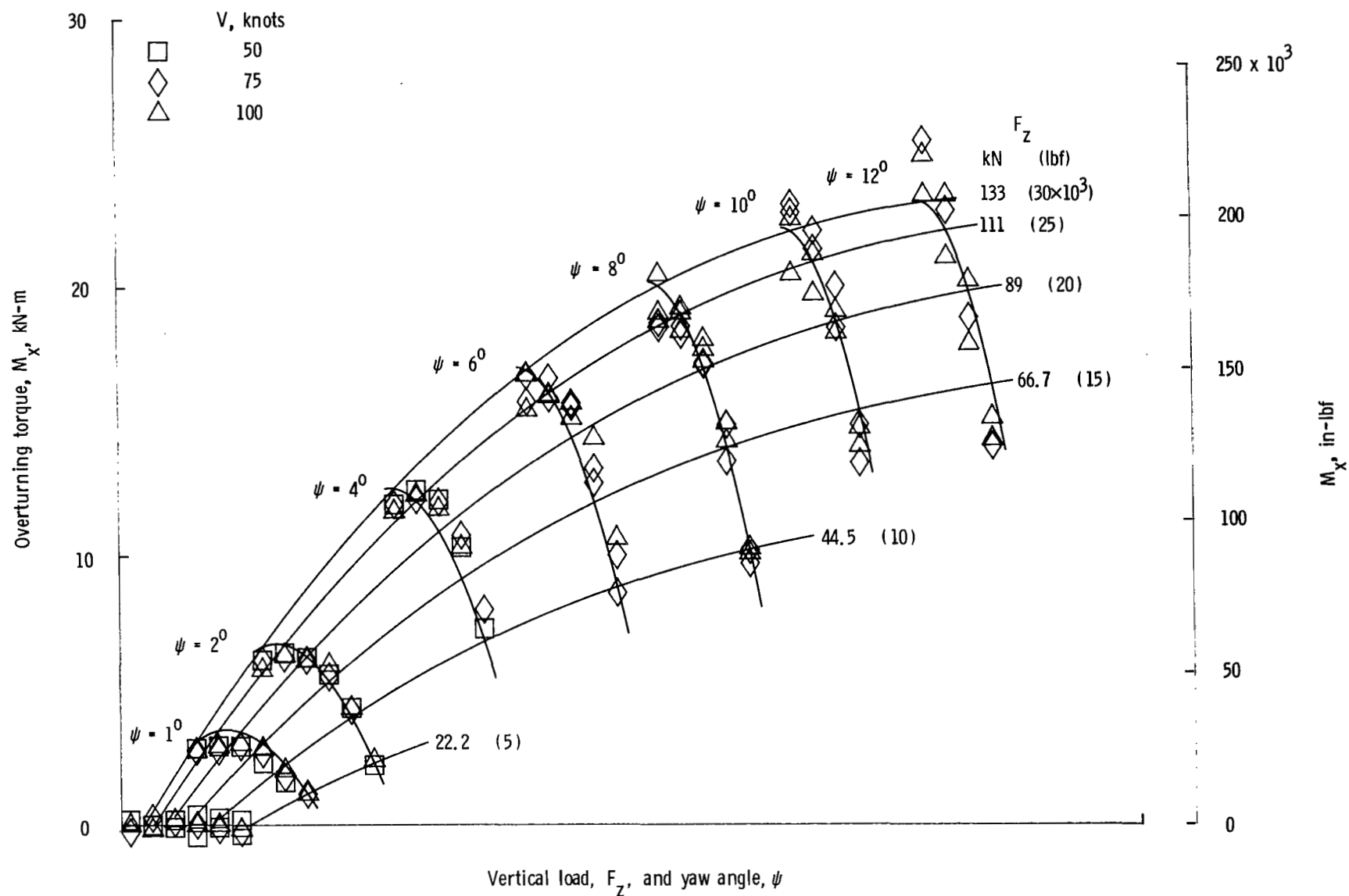


Figure 11.- Variation of overturning torque with vertical load and yaw angle over a range of ground speed.

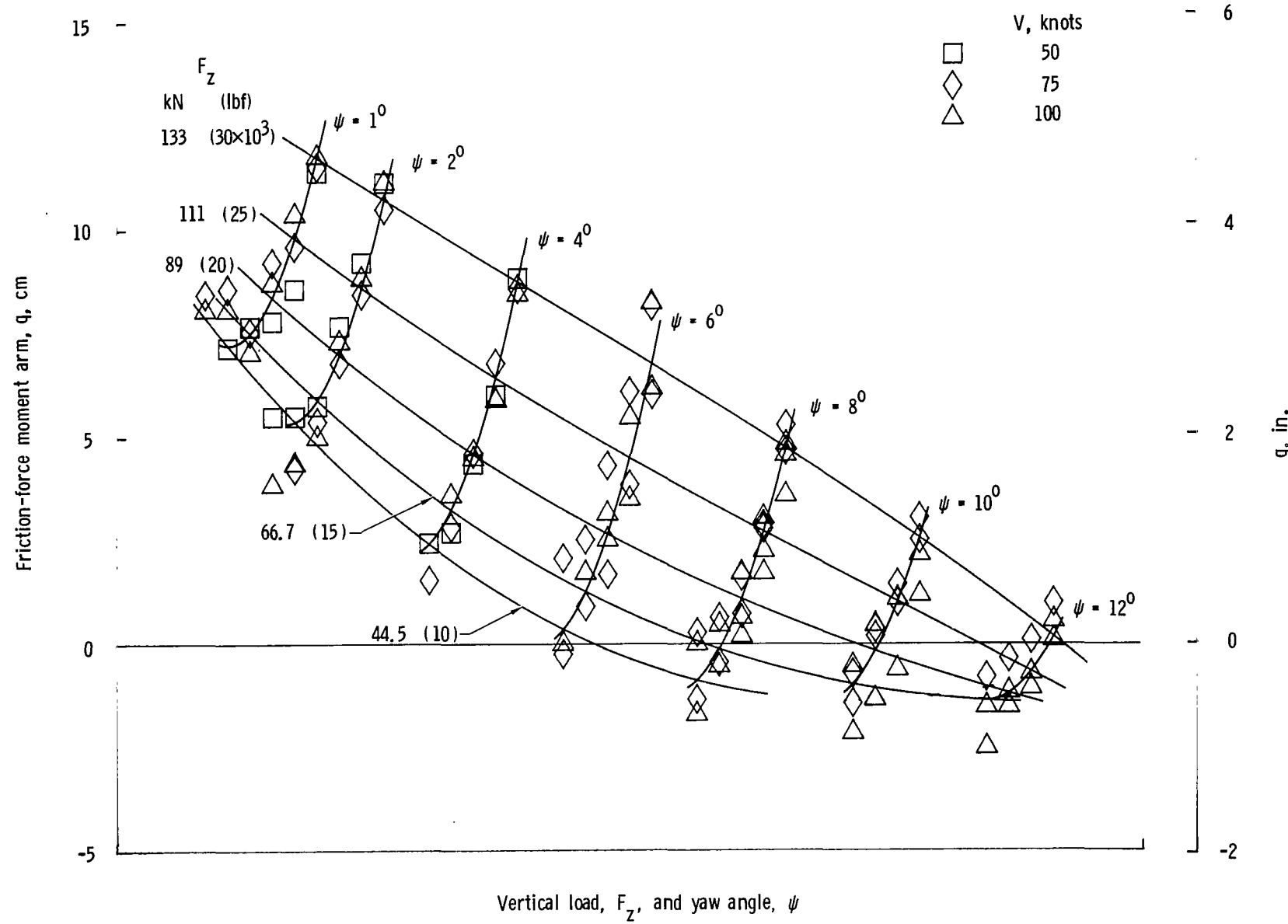


Figure 12.- Variation of friction-force moment arm with vertical load and yaw angle over a range of ground speed.

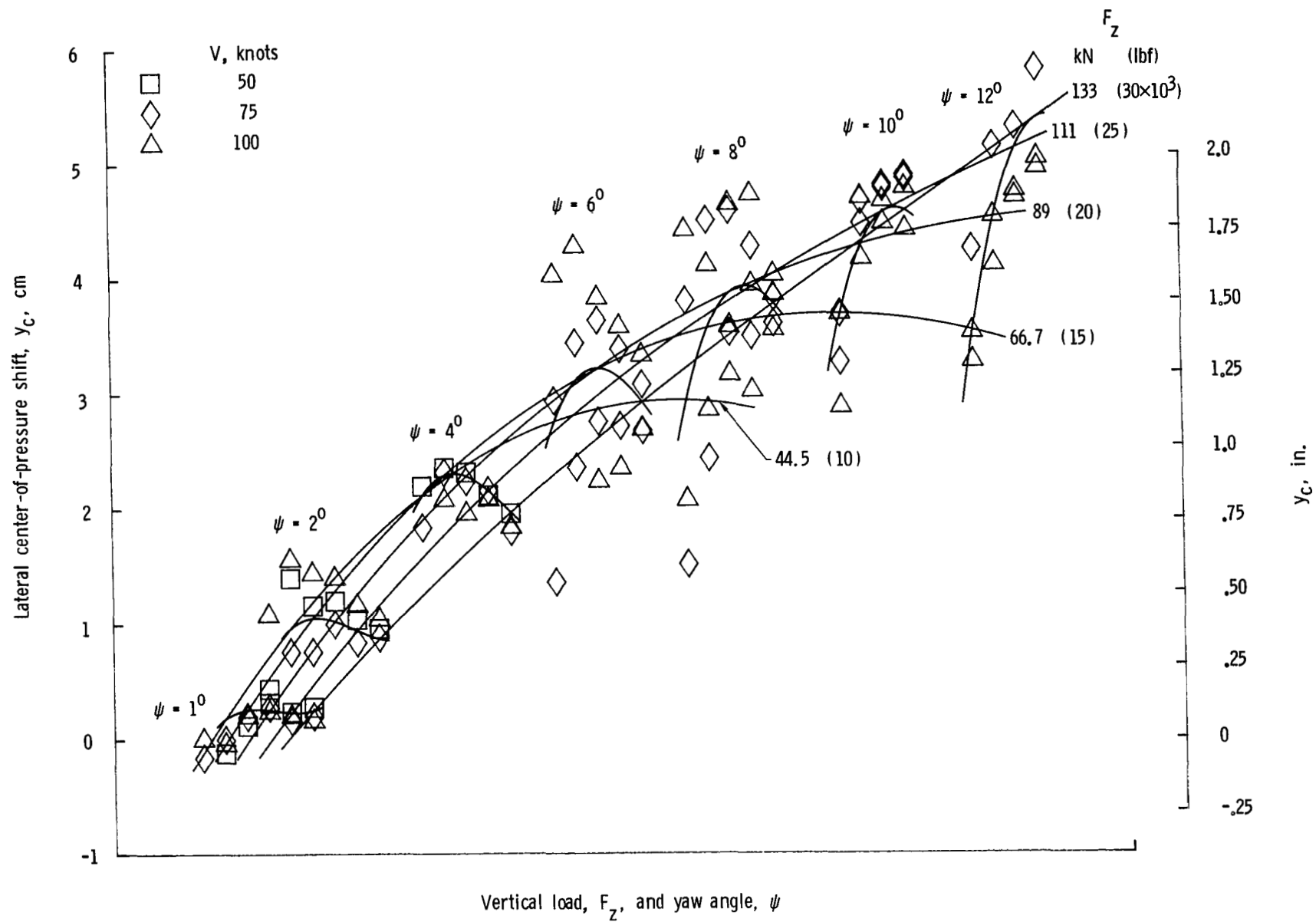


Figure 13.- Variation of lateral center-of-pressure shift with vertical load and yaw angle over a range of ground speed.

1. Report No. NASA TP-1917	2. Government Accession No.	3. Recipient's Catalog No.	
4. Title and Subtitle CORNERING CHARACTERISTICS OF THE NOSE-GEAR TIRE OF THE SPACE SHUTTLE ORBITER	5. Report Date October 1981	6. Performing Organization Code 505-44-33-01	
7. Author(s) William A. Vogler and John A. Tanner	8. Performing Organization Report No. L-14681	10. Work Unit No.	
9. Performing Organization Name and Address NASA Langley Research Center Hampton, VA 23665	11. Contract or Grant No.	13. Type of Report and Period Covered Technical Paper	
12. Sponsoring Agency Name and Address National Aeronautics and Space Administration Washington, DC 20546	14. Sponsoring Agency Code		
15. Supplementary Notes William A. Vogler: Kentron International, Inc., Hampton, Virginia. John A. Tanner: Langley Research Center.			
16. Abstract  An experimental investigation was conducted to evaluate cornering characteristics of the 32 x 8.8 nose-gear tire of the Space Shuttle Orbiter. Data were obtained on a dry concrete runway at nominal ground speeds ranging from 50 to 100 knots and over a range of tire vertical loads and yaw angles which span the expected envelope of loads and yaw angles to be encountered during Space Shuttle landing operations. The cornering characteristics investigated included side and drag forces and friction coefficients, aligning and overturning torques, friction-force moment arm, and the lateral center-of-pressure shift. Results of this investigation indicate that the cornering characteristics of the Space Shuttle nose-gear tire are insensitive to variations in ground speed over the range tested. The effects on cornering characteristics of variations in the tire vertical load and yaw angle are as expected. Trends observed are consistent with trends observed during previous cornering tests involving other tire sizes.			
17. Key Words (Suggested by Author(s)) Nose-gear tire Cornering Mechanical properties	18. Distribution Statement Unclassified - Unlimited	Subject Category 39	
19. Security Classif. (of this report) Unclassified	20. Security Classif. (of this page) Unclassified	21. No. of Pages 27	22. Price A03

For sale by the National Technical Information Service, Springfield, Virginia 22161

National Aeronautics and  
Space Administration

Washington, D.C.  
20546

Official Business  
Penalty for Private Use, \$300

THIRD-CLASS BULK RATE

Postage and Fees Paid  
National Aeronautics and  
Space Administration  
NASA-451



6 110,0, 101381 S00903DS  
DEPT OF THE AIR FORCE  
AF WEAPONS LABORATORY  
ATTN: TECHNICAL LIBRARY (SUL)  
KIRTLAND AFB NM 87117

NASA

POSTMASTER: If Undeliverable (Section 158  
Postal Manual) Do Not Return